Elastic Metamaterial Insulator for Broadband Low-Frequency Flexural Vibration Shielding

Joo Hwan Oh,[1] Shuibao Qi,[2,3] Yoon Young Kim,[4,*] and Badreddine Assouar[2,3,†]

[1]*School of Mechanical, Aerospace and Nuclear Engineering, Ulsan National Institute of Science and Technology, UNIST-gil 50, Eonyang-eup, Ulju-gun,Ulsan 44919, Korea*

[2]*University of Lorraine, Institut Jean Lamour, Boulevard des Aiguillettes, BP: 70239, Vandoeuvre-lès-Nancy 54506, France*

[3]*CNRS, Institut Jean Lamour, Vandoeuvre-lès-Nancy F-54506, France*

[4]*School of Mechanical and Aerospace Engineering, Seoul National University, 599 Gwanak-ro, Gwanak-gu, Seoul 151-744, Korea*

(Received 18 July 2017; revised manuscript received 20 September 2017; published 16 November 2017)

Achieving stop band over broadband at low-frequency range has remained a great scientific challenge in spite of various efforts made using metamaterials or other technologies. In this work, we propose an idea that creates a stop band for broadband at low-frequency range. The dual mechanism of shear stiffening and rotation softening is initiated here to achieve a broad stop band at low-frequency range. Through analytical, numerical, and experimental studies, we reveal the underlying physical mechanism and confirm the effectiveness of this metamaterial on vibration shielding for flexural elastic wave covering 235 to 4520 Hz. This work opens an avenue for the development of elastic metamaterials with performance and functionalities that are highly desirable in many fields such as vibration shielding.

DOI: 10.1103/PhysRevApplied.8.054034

I. INTRODUCTION

Recent advances in acoustic and elastic waves have opened a way to manipulate phonon transfers with artificial media called metamaterials. From the dynamics of artificial unit-cell structures, it was shown that the band gap in quantum scale can also be obtained at the macroscopic scale for wave insulations. The most well-known structure for the wave insulation is a periodic structure mimicking atomic arrangement, called phononic crystals, in which the band gap due to the Bragg scattering can be formed [1–7]. In addition, the resonance-based metamaterials [8–23], of which the effective density or stiffness can be negative around the unit cell's monopolar or dipolar resonance frequencies, have been actively researched. Although these ideas opened a way to insulate and manipulate waves, there are still limitations in the elastic regime in that the broad elastic wave insulation is still hard to be achieved at low-frequency range. There have been several approaches based on the metasurfaces [23–28] and corrugated structures [29–31] for low-frequency wave manipulation, but still the broad band gap at low-frequency range has not been achieved with these ideas. Recently, acoustic [32,33] or elastic [34,35] plasmoniclike phenomena have been reported. However, the acoustic plasmonics cannot be applied to the elastic case due to the physical difference and that elastic plasmonics require an external fixed-boundary condition connected to every unit cell. Also, there has been various research on inertia amplification [36–40], which can provide a very broad stop band at low frequencies. However, it will be much more favorable if one can achieve a broad stop band at any desired frequency ranges with high designability. To clarify this issue, the typical band structure of metamaterials shown in Fig. 1(a) is considered. In phononic crystals, the band gaps are formed at the frequency ranges where the wavelength is comparable with the periodicity of crystal. Therefore, band gaps are usually achieved at high frequencies; i.e., both the lower and upper edge frequencies of the band gap [depicted as ω_1 and ω_2 in Fig. 1(a)] are high. On the other hand, for the band gaps formed by resonance-based metamaterials ω_1 and ω_2 can be low, and a low-frequency band gap can be achieved. However, due to the nature of resonance, the band gaps generally suffer from narrow bandwidth. If attainable, very low ω_1 and very high ω_2 can obviously provide the broad wave insulation at low-frequency range. However, there has been no method enabling such frequency tuning.

In this research, we propose an elastic metamaterial for the elastic wave insulation at broad low-frequency range. The metamaterial proposed in this work, shown in Fig. 1(b), is a periodic structure as in phononic crystals. However, in our metamaterial, the lower and upper edge frequencies of the band gap ω_1 and ω_2 can independently be tuned so that very low ω_1 and very high ω_2 can be

*Corresponding author.
yykim@snu.ac.kr
†Corresponding author.
badreddine.assouar@univ-lorraine.fr

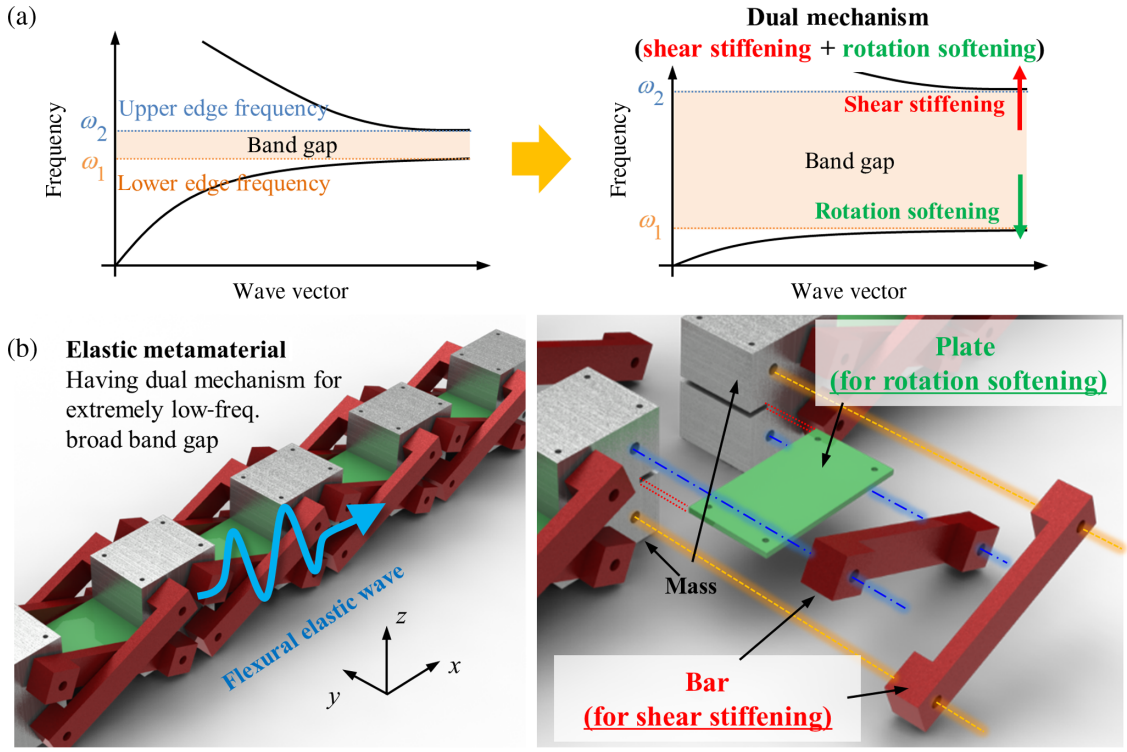

FIG. 1. (a) Schematic illustration of the main idea, dual mechanism of shear stiffening, and rotation softening. (b) The proposed elastic metamaterial with the dual mechanism; the bar provides the shear stiffening, while the plate provides the rotation softening.

simultaneously achieved. Figure 1(a) shows the main idea enabling the frequency tuning: the dual mechanism of shear stiffening and rotation softening. Here, we mainly focus on the elastic wave propagating along thin plate with its polarization along the thickness direction (usually called the flexural wave). Note that the same idea can also be applied to other elastic wave modes if a mass-spring system is properly designed. Unlike in acoustic or electromagnetic waves, the wave motion is governed by two kinds of stiffnesses in flexural elastic wave, i.e., the vertical shear stiffness and the rotational stiffness. We find that the lower edge frequency ω_1 is governed by the rotational stiffness, while the upper edge frequency ω_2 by the shear stiffness. Therefore, increasing shear stiffness (shear stiffening) and decreasing rotational stiffness (rotational softening) can provide the broad stop band at low-frequency range. In our metamaterial consisting of a rigid mass block, a mass-connecting plate, and a set of side bars linking the adjacent mass blocks [41,42], the plate structure is mainly dedicated to the rotational softening, while the bar parts are mainly dedicated to the shear stiffening. Therefore, a very broad band gap at low frequency can be achieved with the proposed metamaterial. Numerical and experimental investigations show that the achieved the band gap extends from 235 to 4520 Hz. Also, the proposed method can provide very high designability, which is very favorable in various applications such as vibration shielding.

II. DUAL MECHANISM OF SHEAR STIFFENING AND ROTATION SOFTENING

A. Key idea in realizing the broad band gap

Because the key idea in realizing the broad band gap at low frequencies is the dual mechanism, we explain why it is critical. Consider a flexural elastic wave propagating through an infinite periodic equivalent mass-spring system with the periodicity of a, as shown in Fig. 2. The model in Fig. 2 reflects the fact that flexural elastic waves are governed by vertical shear stiffness and rotational stiffness;

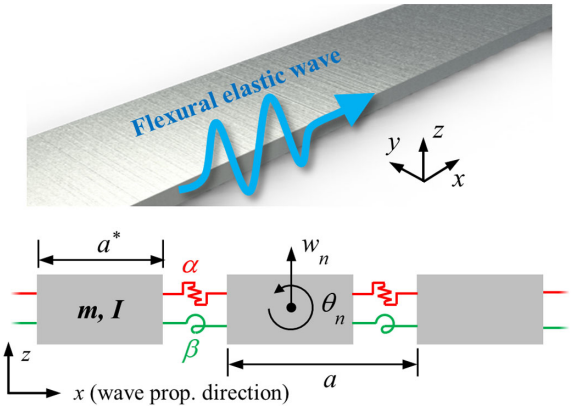

FIG. 2. General mass-spring system of the flexural elastic wave.

the equivalent mass-spring model shown in Fig. 2 [41,43] includes two springs α and β that have vertical shear and rotational stiffnesses, respectively. Following the detailed procedures shown in the Supplemental Material [44], the equation of motion for the equivalent mass-spring system of a continuum structure shown in Fig. 2 is given as

$$-\omega^2\begin{bmatrix} mw_n \\ I\theta_n \end{bmatrix} = \begin{bmatrix} A & B \\ \mathrm{conj}(B) & C \end{bmatrix}\begin{bmatrix} w_n \\ \theta_n \end{bmatrix}, \tag{1a}$$

where matrix components A, B, and C are defined as

$$A = \alpha[\exp(-ika) + \exp(ika) - 2], \tag{1b}$$

$$B = 0.5a^*\alpha[\exp(ika) - \exp(-ika)], \tag{1c}$$

$$C = \beta[\exp(-ika) + \exp(ika) - 2] - (0.5a^*)^2\alpha[\exp(-ika) + \exp(ika) + 2]. \tag{1d}$$

Based on Eq. (1), one can calculate the lower edge frequency ω_1 and the upper edge frequency ω_2. Since ω_1 corresponds to the wave vector of $ka = \pi$, ω_1 can be analytically calculated by solving Eq. (1) for ω at $ka = \pi$ and selecting the lower one. In the same manner, ω_2 corresponds to the wave vector of $ka = 0$ (if the optical branch has a positive wave speed) or $ka = \pi$ (if the optical branch has a negative wave speed) and, thus, can be analytically calculated by solving Eq. (1) at $ka = 0$ or $ka = \pi$ and selecting the higher one. The calculated results are

$$\omega_1 = 2\sqrt{\beta/I}, \tag{2a}$$

$$\omega_2 = a^*\sqrt{\alpha/I} \quad \text{if } \omega_2 \text{ corresponds to the wave vector of } ka = 0, \tag{2b}$$

$$= 2\sqrt{\alpha/m} \quad \text{if } \omega_2 \text{ corresponds to the wave vector of } ka = \pi. \tag{2c}$$

From Eq. (2), one can clearly see that the lower edge frequency of the band gap ω_1 is a function of β, while the upper edge frequency of the band gap ω_2 is a function of α. To achieve a broad band gap at low frequency, ω_1 should be low, while ω_2 is high; i.e., a small value of β and a large value of α are needed to form a broad band gap in a low-frequency range.

In general continuum media or structures, however, α and β usually increase or decrease simultaneously depending on the thickness, width, and Young's modulus of the continuum medium. Thus, if one lowers β, α also becomes lowered, not increasing the band-gap width. This intrinsic coupling behavior makes it difficult to achieve a broad band gap in a low-frequency range for flexural elastic waves. This is why a new metamaterial is required; a dual-mechanism metamaterial possessing very high α (shear stiffening) and very low β (rotation softening) simultaneously can achieve an extremely broad band gap at low-frequency range.

B. Metamaterial proposition for the dual mechanism

To explain how the dual mechanism can be achieved, we first consider the metamaterial without bar structures shown in the left side of Fig. 3(a). Here, the plate acts as the springs, and the corresponding spring coefficients β_{plate} and

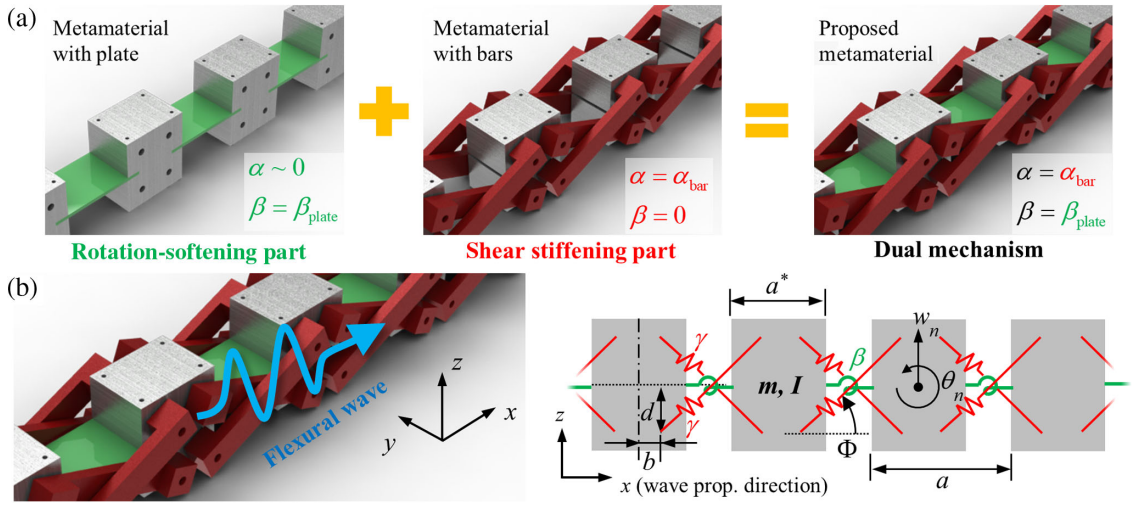

FIG. 3. (a) Design of the proposed elastic metamaterial by combining metamaterial with the plate and that with bars. (b) Equivalent mass-spring system of the proposed elastic metamaterial for the analytic investigation of the proposed metamaterial.

α_{plate} are very small due to its thin thickness. As a result, with the metamaterial without bar structure, the lower edge frequency of the band gap ω_1 is very low due to the small value of β_{plate}; i.e., the rotation softening can be achieved. However, the broad wave insulation at low-frequency range cannot be achieved since the upper edge of the band gap ω_2 is also very low due to the very small value of α_{plate}, and, thus, the band gap is very narrow.

Now, consider the metamaterial without plate structure shown in the middle of Fig. 3(a). As shown in the previous research, the metamaterial with the crossed hinge-connected bar structure has zero rotational stiffness $\beta_{\text{beam}} = 0$ but nonzero vertical stiffness α_{beam} [41]. Accordingly, the shear stiffening can be achieved by increasing the bar's stiffness; if the bar structure has very high stiffness, the upper edge frequency of the band gap ω_2 will be very high. Also, the lower edge frequency ω_1 remains almost zero value due to the zero rotational stiffness. Unfortunately, it shows that the metamaterial structure having zero rotational stiffness cannot sustain its own weight under the static case, and, thus, it is extremely hard to apply the metamaterial in actual applications. Also, the metamaterial without the plate structure does not have any mechanism to tune the lower edge frequency of the band gap. The metamaterial without the plate structure cannot realize the broad wave insulation at low-frequency range.

Finally, by combining two metamaterials as in the right of Fig. 3(a), a metamaterial with rotational stiffness $\beta = \beta_{\text{plate}}$ and vertical shear stiffness $\alpha = \alpha_{\text{plate}} + \alpha_{\text{beam}} \sim \alpha_{\text{beam}}$ (since $\alpha_{\text{beam}} \gg \alpha_{\text{plate}}$) can be achieved. In this metamaterial, the plate provides low rotational stiffness (rotation softening), while the bars provide high vertical shear stiffness (shear stiffening). This point indicates that each stiffness component can be independently tuned to have very low ω_1 and very high ω_2. Therefore, a broad band gap at very low-frequency range can be obtained. Furthermore, each frequency can be independently tuned by adjusting the plate and the bar structure, respectively, to obtain any range of band gap.

This point can be better explained if the equivalent mass-spring system is analytically investigated, as shown in Fig. 3(b). In Fig. 3(b), the spring coefficient γ originates from the stiffness of the connecting bar, while the rotational spring coefficient β from the bending stiffness of the connecting plate. As a result, the wave dispersion relationship can be expressed as (see the Supplemental Material for details [44])

$$-\omega^2 \begin{bmatrix} mw_n \\ I\theta_n \end{bmatrix} = \begin{bmatrix} A' & B' \\ \text{conj}(B') & C' \end{bmatrix} \begin{bmatrix} w_n \\ \theta_n \end{bmatrix}, \tag{3a}$$

$$A' = 2\gamma \sin^2\Phi[\exp(-ika) + \exp(ika) - 2], \tag{3b}$$

$$B' = 2\gamma \sin\Phi(b\sin\Phi + d\cos\Phi)[\exp(ika) - \exp(-ika)], \tag{3c}$$

$$C' = \beta[\exp(-ika) + \exp(ika) - 2] - 2\gamma(b\sin\Phi + d\cos\Phi)^2[\exp(-ika) + \exp(ika) + 2], \tag{3d}$$

where Φ is the angle of the bar structure as shown in Fig. 3. Comparing Eq. (3) with Eq. (1), the following equivalences can be observed:

$$\alpha = 2\gamma\sin^2\Phi, \quad a^* = 2(b\sin\Phi + d\cos\Phi)/\sin\Phi, \quad \beta = \beta. \tag{4}$$

Equation (4) reveals a very important fact: the bar stiffness γ affects only the shear spring coefficient α, while the plate's stiffness affects the rotational spring coefficient β. Therefore, the proposed metamaterial can have the dual mechanism of shear stiffening and rotation softening by designing the metamaterial with small β and considerably large α, from which the extremely broad band gap in low-frequency range can be achieved. It should be noted that there should be a certain lower limit for the rotational spring coefficient β, otherwise, the metamaterial will not sustain its own weight.

It should be noted that the equivalent mass-spring system shown in Fig. 3(b) can be used only for low-frequency ranges because the mass of the bar and plate are not considered. At high frequencies, it is shown that the bar or plate can exhibit dynamic motions due to their own mass, and the equivalent mass-spring model shown in Fig. 3(b) fails to describe the wave motion of the metamaterial. For instance, at frequencies around 6500 Hz, it is shown that the bar structure is under the resonance motion so that other forces that are not considered in the mass-spring system in Fig. 3(b) take place. However, at low frequencies, as in this work, it is shown that the plate and bar structures are almost in their quasistatic motion, and those masses can be ignored.

III. NUMERICAL VALIDATION

A. Validation of the idea with wave dispersion curves

Based on the analytic investigation, numerical simulations are carried out to validate our idea. The wave dispersion curve of the proposed elastic metamaterial is numerically and analytically calculated. In the numerical simulation, the unit-cell structure shown in Fig. 4(a) is used, the Floquet-Bloch boundary condition (periodic BC) [5] is imposed at the sides of the unit cell, and the eigenvalue problem is solved for various wave vectors k inside the first Brillouin zone [45,46]. In particular, the

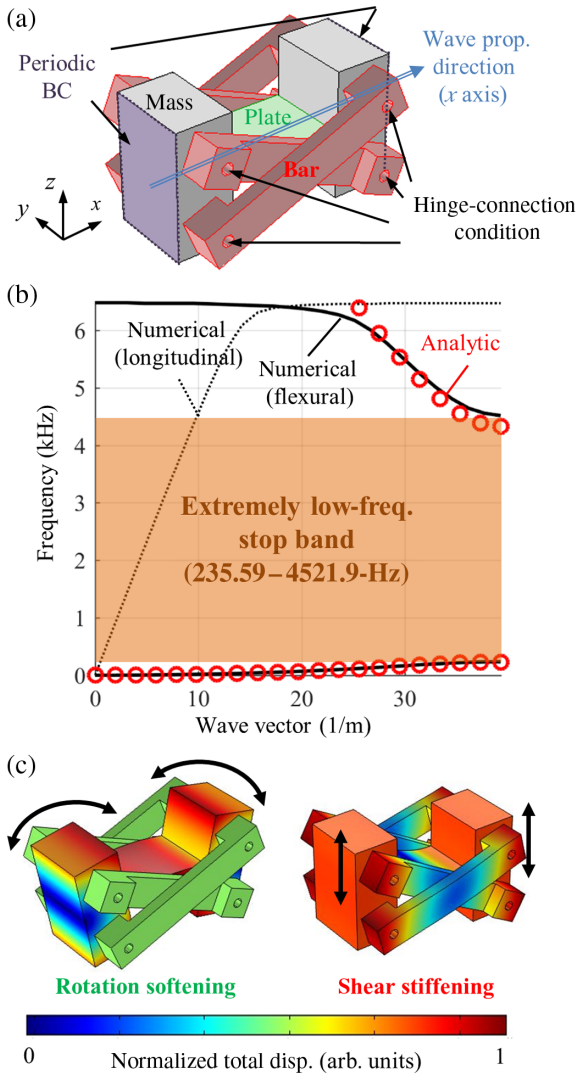

FIG. 4. (a) A unit-cell structure of the proposed elastic metamaterial considered in the numerical simulation. (b) The numerically and analytically calculated wave dispersion curves. (c) Mode shapes of the unit-cell structure at the lower (left) and upper (right) edge of the band gap, respectively.

hinge connection should be properly considered in the simulation. For the analytic calculation, the spring and mass coefficients of the actual metamaterial are analytically or numerically determined to obtain the analytic dispersion curve by using the mass-spring model. The detailed geometry, material properties, and calculation procedure are given in the Supplemental Material [44].

The dispersion curve in Fig. 4(b), which is obtained for the proposed metamaterial, supports our argument that the proposed metamaterial effectively forms a broad band gap at low frequencies, specifically, between 235.59 and 4521.9 Hz. The normalized bandwidth is 1.802. Also, very good agreement can be observed between the analytically calculated wave dispersion curves and the numerically calculated one, validating our analytic approaches based on the equivalent mass-spring system. In addition, the formation of broad band gap at low frequencies from 235.59 to 4521.9 Hz clearly supports that our idea of the dual mechanism works well as desired.

Since the metamaterial is not symmetric along the thickness direction (due to the bar connection), one may argue that there may exists a coupling between the longitudinal (x-polarized) and flexural (z-polarized) waves. Thus, in Fig. 4(b), both the wave dispersion curves for longitudinal (x-polarized) and flexural (z-polarized) waves are plotted, while other wave modes such as the shear (y-polarized) and torsional (rotation with respect to the x axis) are not plotted due to the unit cell's symmetric configuration. As can be seen in the dispersion curve, the coupling effect between the longitudinal and flexural waves does not affect the overall wave dispersion curves at the frequency range of interest. In fact, although the bar structures are not symmetric along the z direction, the coupling effect is shown to be almost negligible.

Figure 4(c) shows the mode shapes of the unit-cell structure at the lower and upper edge frequency of the band gap, respectively. As can be seen in Fig. 4(c), the mode shape at the lower edge of the band gap (left) is dominated by the rotational motion of the mass block, while that of the upper edge (right) is dominated by the vertical motion of the mass block. This agrees well with our findings shown in the previous section that the lower edge frequency of the band gap is governed by the rotational stiffness, while the upper edge frequency is governed by the vertical shear stiffness. Also, it can be seen that at the lower edge of the band gap, the plate exhibits large displacements, while the bars do not show any displacement. This supports that the rotation softening is mainly from the plate structure. On the other hand, at the upper edge frequency both the plate and bars exhibit large displacements because the plate also has a vertical shear stiffness. However, since the plate's vertical shear stiffness is very small, it does not highly affect the shear-stiffening mechanism. More simulation results with various plate and bar stiffnesses are given in the Supplemental Material [44].

B. Numerical simulation for the low-frequency wave insulation

Figure 5(a) is the numerical simulation setting to measure the flexural wave transmission of the proposed elastic metamaterial. For the simulation, we use the metamaterial system consisting of four unit cells arranged along the x direction. The fixed condition is imposed at the left boundary of the system, and the vertical harmonic force is applied at the second mass, as indicated in Fig. 5(a). Under this condition, the time harmonic simulation is carried out for various frequencies. In addition, only half of the system is modeled, and the symmetric boundary condition along the y direction is imposed to reduce the computational time.

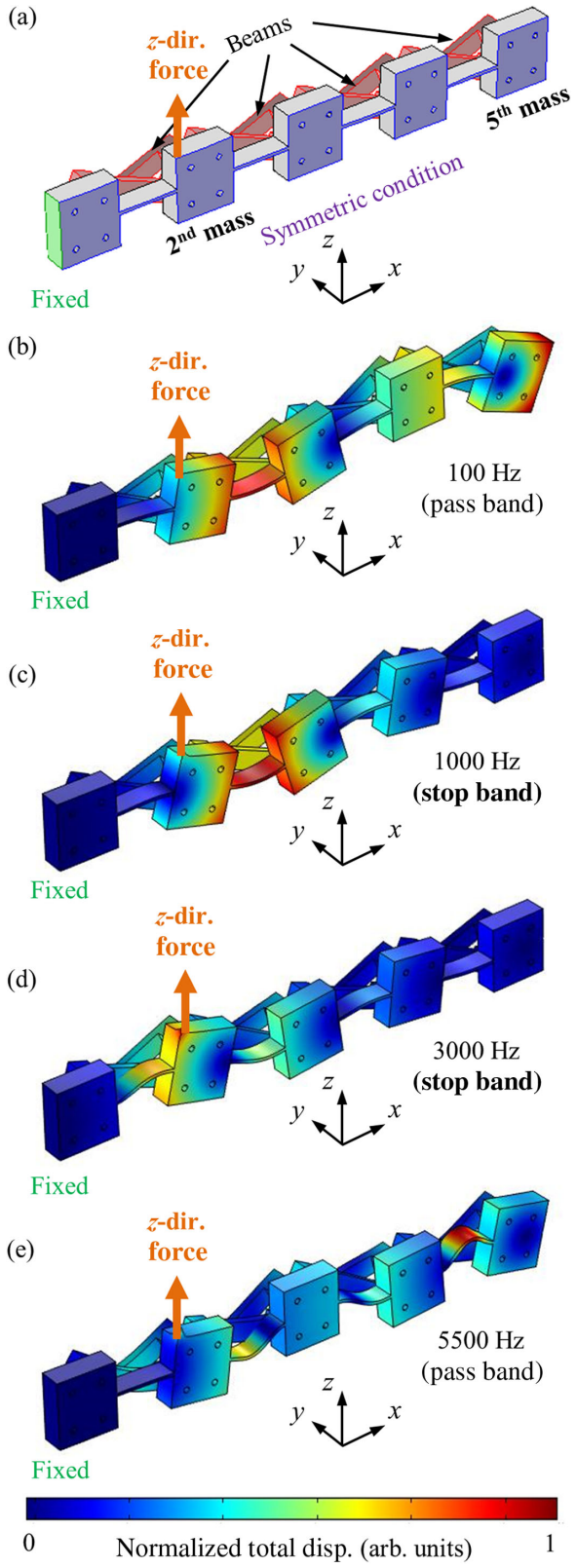

FIG. 5. (a) The metamaterial system considered in the numerical simulation. The simulation results for (b) 100 Hz, (c) 1000 Hz, (d) 3000 Hz, and (e) 5500 Hz.

It should be noted that the simulation setting in Fig. 5(a) is not generally used in measuring the wave transfer in metamaterial; generally, wave-based simulations (using the perfectly matched layers or finite-difference time-domain method) are considered to measure the wave transfer in the metamaterials. However, in this work, the simulation setting in Fig. 5(a) is used to correlate the simulation with the experiment; the reasons why such a setting is required in experiment are explained later in the paper. Nevertheless, the simulation carried out in this work can also be useful to predict the formation of the band gap; if an actuating frequency belongs to the band gap, there will be no wave transfer, and the harmonic motion of the fifth mass in Fig. 5(a) should be very low, too.

Figures 5(b)–5(e) show the simulation results for various frequencies of 100, 1000, 3000, and 5500 Hz. At 100 Hz (which belongs to the pass band), both second and fifth masses exhibit large vibration, indicating that there exists wave transfer between each mass. However, at 1000 and 3000 Hz (which belong to the band gap), the fifth mass exhibits very small vibration compared with the second mass. This shows that the wave transfer is highly suppressed, and very small wave transfer exists between each mass; i.e., the band gap is formed to suppress the wave transfer. At 5500 Hz (which belongs to the pass band), the fifth mass vibrates again and shows the rotational motion again, indicating that the frequency belongs to the pass band.

To better observe the flexural wave insulation at various frequencies, the vibration transmission is measured for various frequencies by normalizing the motion of the fifth mass with that of the second mass. To calculate the vibration transmission, the vertical displacement at the left and right sides of the second and fifth masses are measured for varying excitation frequencies, respectively. Then, the rotations of the second and fifth masses are calculated and normalized to evaluate the vibration transmission plotted in Fig. 6(b). It should be noted that unlike in the general wave simulation, the ratio can exceed 1 since it is based on the vibration simulation. Figures 6(b) clearly demonstrates that the vibration transmission is extremely low in the frequency range of 235 to 4520 Hz. This behavior is consistent with the formation of the broad band gap at low frequency for the flexural elastic wave, as predicted by the dispersion curve. Such low vibration is almost impossible to achieve with general materials such as viscoelastic materials; see the simulation results shown in the Supplemental Material [44] that compares the vibration shielding performance of the proposed metamaterial and the conventional rubber beam. This low vibration transmission can be effectively applied in various applications on vibration shielding.

To check whether the stop-band frequencies are highly affected by the damping effect, Fig. 6(b) is prepared with

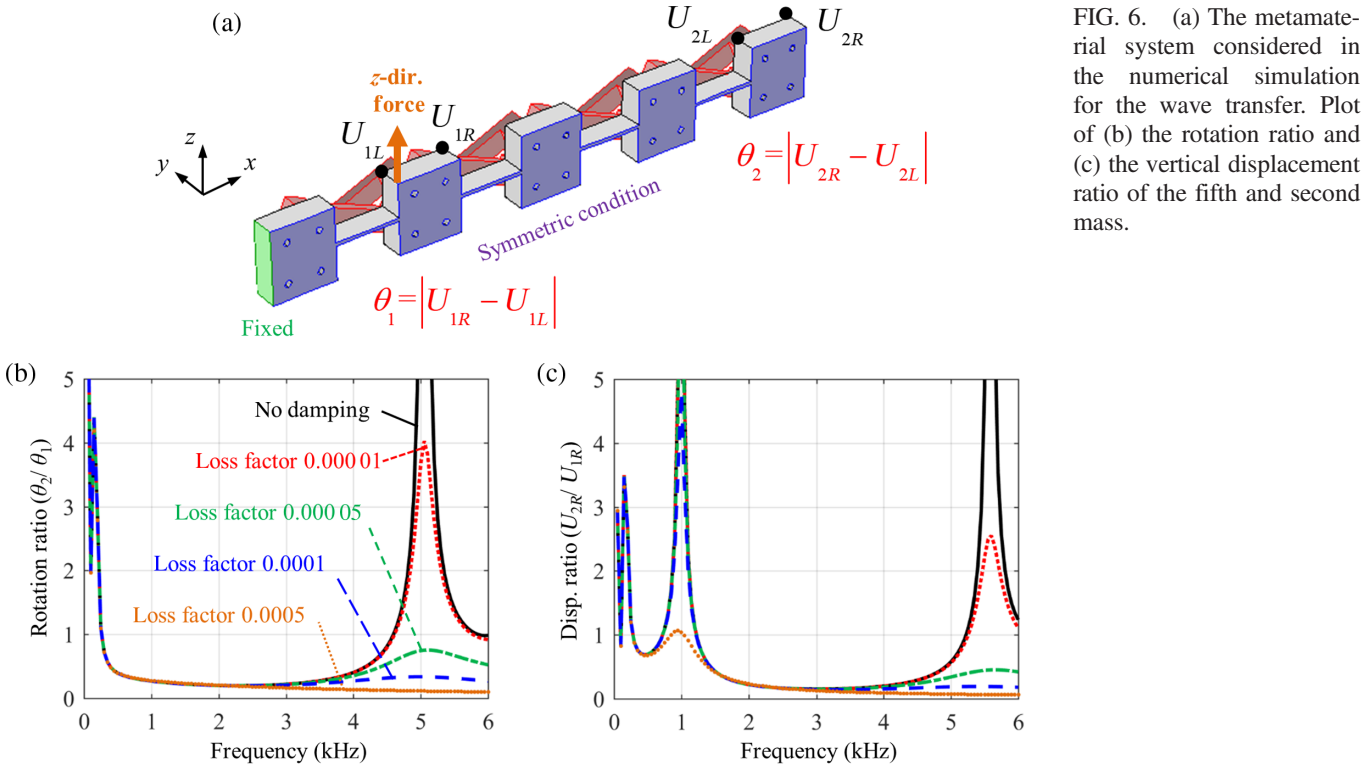

FIG. 6. (a) The metamaterial system considered in the numerical simulation for the wave transfer. Plot of (b) the rotation ratio and (c) the vertical displacement ratio of the fifth and second mass.

the transmission under various damping coefficients. Figure 6(b) shows that the transmission behavior and the stop-band frequencies are little affected by the effect of damping, suggesting the robustness of the proposed metamaterial system for the lossy cases.

Note that instead of the rotation of each mass, the vertical displacement may also be considered to evaluate the wave transfer since the flexural wave is governed by both vertical and rotational motion. However, since we consider the vibration simulation with the fixed boundary condition here, the use of vertical displacement may cause a wrong result. Figure 6(c) shows the vibration transmission measured for the ratio of vertical motion. In Fig. 6(c), there seems to be a pass band around 1000 Hz, which, in fact, belongs to the band gap as shown in Fig. 5(c). This is mainly because of the fixed boundary condition imposed at the left side of the metamaterial structure; due to the fixed boundary, the second mass exhibits large rotation but very small vertical displacement at 1000 Hz. In fact, the rotational motion is more dominant than the vertical one in the low-frequency ranges, as elucidated in the literature [41,43,45].

IV. EXPERIMENTAL REALIZATION

A. Experimental setting

We fabricate the metamaterial system and carry out the experiment as shown in Fig. 7. Aluminum material is used to make all components (masses, bars, rods, and plates) of the metamaterial, and the bars are assembled to the mass block by rods to form the hinge connection. The fabrication details of the metamaterial can be found in the Supplemental Material [44].

The experiment is set up to simulate the conditions used for the numerical simulation depicted in Fig. 6(a); the left side is the fixed piezoelectric actuator installed at the second mass. Note that the static deformation of the metamaterial sample is shown to be less than 0.1 mm, which can be ignored in the experiments. At the piezoelectric actuator, the sine wave is actuated with various frequencies from 0.1 to 6 kHz. After the actuation, the displacement of each mass is measured with the laser Doppler vibrometer (PSV-500). In the measurement, the following sampling frequencies are used for each frequency range to achieve the best results: 12.5 kHz from 0.1 to 1 kHz, 50 kHz from 1 to 4 kHz, and 100 kHz from 4 to 6 kHz. Also, the measurements are carried out at the left and right side of the second and fifth mass, respectively, to measure the rotation of each mass, as in the simulation. After the measurement, the Fourier transformation is carried out to extract the displacement amplitude at the actuating frequency.

It is worth noting that the general experiments are carried out as follows: Actuation is made at the media outside the metamaterial, and the reflected and transmitted waves are measured at the outside media with proper methods. However, in this work, we find that the general wave experiments are hard to apply and may not be accurate. The most critical problem is that in such a thick plate, the actuation is not strong enough that it requires some time to have enough amplitude. Since there exist very small gaps

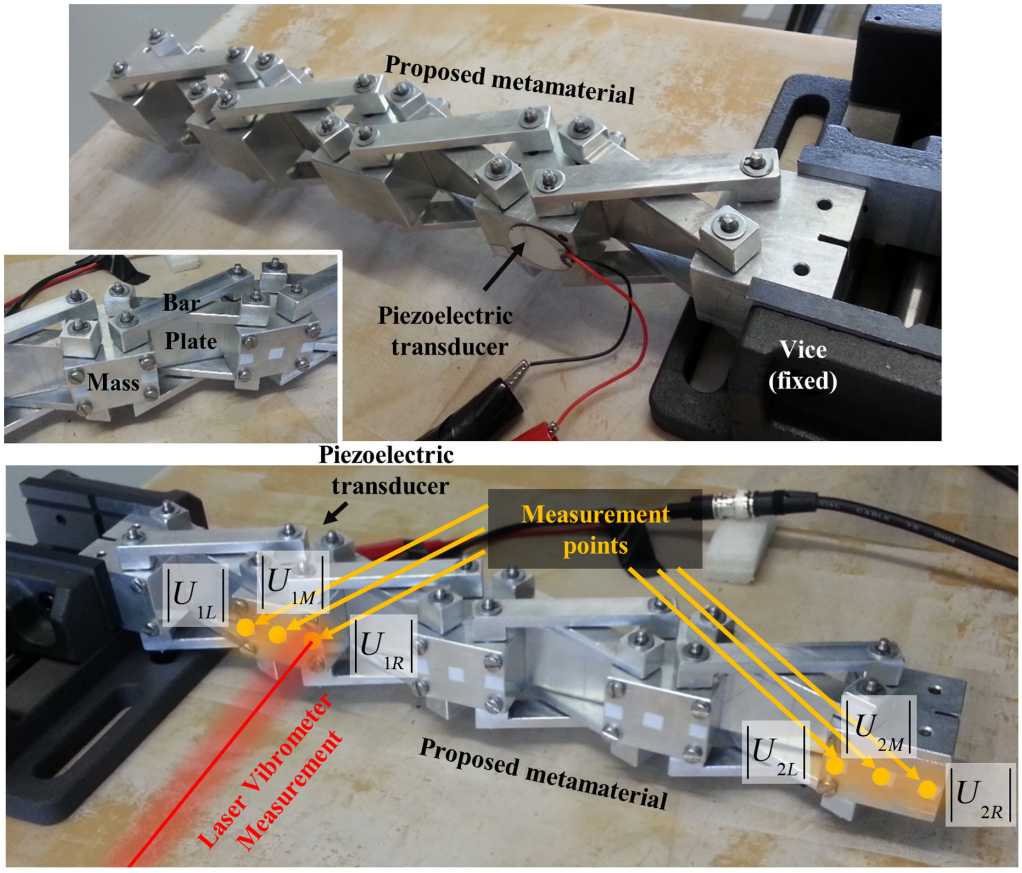

FIG. 7. Experimental setting for the realization of wave insulation with the proposed elastic metamaterial.

between mass and rod (or rod and bar), small excitation may result in zero wave transmission, regardless of the frequency. On the other hand, in our vibration experiment, the measurements are carried out under the steady state, and there is enough time for sufficient energy transferring into the metamaterial. Therefore, sufficiently large actuation and fully developed flexural waves inside the metamaterial can be achieved with the current vibration experiment. Although this experiment cannot provide any other data such as effective parameters or dispersion curve of the metamaterial, it can accurately show the formation of a band gap, which is the main point focused on in this work.

After the measurement, the rotation of the second and fifth masses is calculated. Unlike the case of simulation, special attention is required here. In the simulation, the rotation of each mass can be readily calculated as $\theta = |U_R - U_L|$. However, since the Fourier transformation used in the experiment provides amplitudes for each frequency component, the experimentally measured values are always positive, i.e., $|U_R|$ and $|U_L|$ are measured. Thus, if we calculate the rotation with the difference between the measured values at the left and right side, the result is $|U_R| - |U_L|$, which causes a problem if the displacements at the left and right side have different sign. Therefore, we additionally measure the displacement at the middle of the mass U_M in Fig. 7. If the average of the measured value is similar to U_M, $|U_R| + |U_L| \sim 2|U_M|$, U_R and U_L have the same sign, and the rotation can be defined as $\theta = |U_R| - |U_L|$. However, if the average is larger than U_M, $|U_R| + |U_L| > 2|U_M|$, U_R and U_L have the different sign, and the rotation should be defined as $\theta = |U_R| + |U_L|$. Note that no other exceptional case is observed since the mass exhibits almost rigid-body motion.

B. Experimental results

Figure 8(a) compares the rotation ratios (calculated by the ratio of the rotation of the fifth mass to that of the second mass) that are obtained numerically and experimentally. Here, the +, o, and × markers indicate the experimental results obtained for different sampling rates. As previously explained, three different sampling rates are used in the experiments since the target frequency range is very broad, and a single sampling rate cannot be used: 12.5 kHz from 0.1 to 1 kHz (corresponding to the + marker), 50 kHz from 1 to 4 kHz (corresponding to the o marker), and 100 kHz from 4 to 6 kHz (corresponding to the × marker). To consider any possible loss effect, the experimentally measured loss factor of $1.62e-8 \times f$, where f is the actuation frequency, is used in the simulation.

Even though there are some discrepancies, they agree well in the targeted band-gap frequency range (235 to 4520 Hz), validating the actual formation of such a broad band gap at low-frequency range. At extremely low frequencies, from 0 to 300 Hz, high vibration transmission

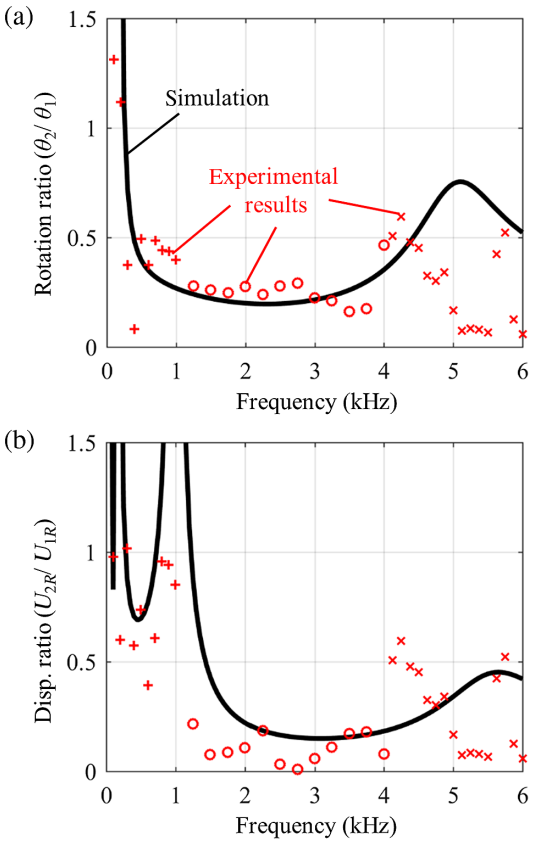

FIG. 8. Experimentally measured wave transfer in the proposed elastic metamaterial at various frequencies. Plot of (a) the rotation ratio and (b) the vertical displacement ratio of the fifth and second mass.

can be observed, indicating that those frequencies belong to the pass band of the metamaterial. On the other hand, at frequencies from 300 to 4000 Hz, the vibration transmission becomes significantly lowered. This is due to the formation of the stop band, as in the simulation, the formation of the stop band prohibits the flexural wave propagation, and, thus, a very small amount of the vibration is transferred from the actuation point (the second mass) to the measurement point (the fifth mass). Finally, at frequencies higher than 4000 Hz, high vibration transmission is measured, indicating that the frequency range corresponds to the pass band of the metamaterial. Overall, the experiment well captures the broad band gap at low frequencies as predicted by the simulation.

The discrepancy between the experimental result and the simulation result can be found around 5000 Hz, which is caused by the effect of the rods' deformation ignored in simulations. Since almost all regions of the rod are embedded in other parts, the deformation of the rod is mainly a shear one at a very small region, indicating that the stiffness of the rod is very high. Furthermore, because almost all deformation takes place at a plate structure at low frequencies, the stiffness of the rod can be ignored at low frequencies. However, at high frequencies where the deformation of the bar becomes dominant, the stiffness effect of the rod also affects the overall motion. The peaks in Fig. 8(a) are due to the formation of the standing wave mode inside the metamaterial (since the simulations and experiments are carried out under the steady state), and the stiffness of the aluminum rod decreases the overall stiffness, resulting in the reduced peak frequency in the experimental results. The discrepancy can be reduced if the stiffness of the rod becomes significantly harder than the bar. For instance, if the bar is made of plastic or if the rod is made of steel, the experimental result will fit much better.

In addition to the rotation ratio, the vertical displacement ratio is also experimentally calculated and compared in Fig. 8(b). Good agreement can be observed in the case of the displacement ratio, which well supports the validity of the experimental results.

V. DISCUSSION

In this research, we propose an idea of wave insulation for the broad- and low-frequency range by the dual mechanism of shear stiffening and rotation softening. Based on our idea, we create an elastic metamaterial with a configuration of a rigid mass block, a thin mass-connecting plate, and a set of bars that are hinge connected to the masses. The analytic investigation shows that the plate alone contributes to the lower edge of the band gap by rotation softening, while the bars largely contribute the shear stiffening that governs the upper band-edge frequency. Numerical and experimental results show that the realized band gap is from 235 to 4520 Hz. Although the numerical and experimental validations are carried out for one-dimensional flexural elastic waves, the idea can also be extended to other wave modes and to a two- or three-dimensional system. In fact, the idea can also be applied for other wave modes such as the longitudinal or shear wave mode if a unit cell is properly designed so that the longitudinal or shear motion is coupled with additional rotational motion.

As possible applications, our idea of the shear stiffening and rotational softening can effectively be applied in various vibration shielding applications. Usually, in vibration shielding, it has been a long issue to effectively isolate vibration at very low and broad frequencies. Moreover, almost all vibration problems are based on the flexural motions. Our metamaterial can provide extremely effective broadband flexural vibration shielding at very low-frequency ranges, which cannot be achieved with general materials. Since the lower and upper edge frequencies of the stop band can be easily tuned, our idea can be readily applied in various applications such as vibration reduction in bridges or buildings, vibration engineering in cars, automobile applications, etc. Furthermore, various vibration devices can be designed, such as vibration waveguides, cavities, and vibration focusing based on the present research. We believe that our metamaterial will open a way for flexural vibration manipulation at low-frequency ranges.

ACKNOWLEDGMENTS

This work is supported by the Center for Advanced Meta-Materials (CAMM) funded by the Ministry of Science, ICT and Future Planning as Global Frontier Project (Grant No. CAMM-2014M3A6B3063711), by the National Research Foundation of Korea grant funded by the Korea government (MSIP) (Grant No. 2017R1C1B1004436), and by the Institut CARNOT—ICEEL (France). The authors thank Emmanuel Vatoux for the structures fabrication.

[1] M. Sigalas and E. N. Economou, Band structure of elastic waves in two dimensional systems, Solid State Commun. **86**, 141 (1993).

[2] M. S. Kushwaha, P. Halevi, L. Dobrzynski, and B. Djafari-Rouhani, Acoustic Band Structure of Periodic Elastic Composites, Phys. Rev. Lett. **71**, 2022 (1993).

[3] J. H. Lee, C. Y. Koh, J. P. Singer, S. J. Jeon, M. Maldovan, O. Stein, and E. L. Thomas, 25th anniversary article: Ordered polymer structures for the engineering of photons and phonons, Adv. Mater. **26**, 532 (2014).

[4] E. Yablonovitch, Inhibited Spontaneous Emission in Solid-State Physics and Electronics, Phys. Rev. Lett. **58**, 2059 (1987).

[5] L. Brillouin, *Wave Propagation in Periodic Structures* (Dover Publications, Inc., New York, 1946).

[6] S. Babaee, N. Viard, P. Wang, N. X. Fang, and K. Bertoldi, Harnessing deformation to switch on and off the propagation of sound, Adv. Mater. **28**, 1631 (2016).

[7] N. Garcia, M. Nieto-Vesperinas, E. V. Ponizovskaya, and M. Torres, Theory for tailoring sonic devices: Diffraction dominates over refraction, Phys. Rev. E **67**, 046606 (2003).

[8] Z. Liu, X. Zhang, Y. Mao, Y. Y. Zhu, Z. Yang, C. T. Chan, and P. Sheng, Locally resonant sonic materials, Science **289**, 1734 (2000).

[9] H. H. Huang, C. T. Sun, and G. L. Huang, On the negative effective mass density in acoustic metamaterials, Int. J. Eng. Sci. **47**, 610 (2009).

[10] Z. Hou and B. M. Assouar, Tunable solid acoustic metamaterial with negative elastic modulus, Appl. Phys. Lett. **106**, 251901 (2015).

[11] R. Zhu, X. N. Liu, G. K. Hu, C. T. Sun, and G. L. Huang, A chiral elastic metamaterial beam for broad band vibration suppression, J. Sound Vib. **333**, 2759 (2014).

[12] M. Oudich, M. Senesi, M. B. Assouar, M. Ruzzene, J. H. Sun, B. Vincent, Z. Hou, and T. T. Wu, Experimental evidence of locally resonant sonic band gap in two-dimensional phononic stubbed plates, Phys. Rev. B **84**, 165136 (2011).

[13] E. G. Williams, P. Roux, M. Rupin, and W. A. Kuperman, Theory of multiresonant metamaterials for A0 Lamb waves, Phys. Rev. B **91**, 104307 (2015).

[14] V. Romero-Garcia, A. Krynkin, L. M. Garcia-Raffi, O. Umnova, and J. V. Sanchez-Perez, Multi-resonant scatterers in sonic crystals: Locally multi-resonant acoustic metamaterial, J. Sound Vib. **332**, 184 (2013).

[15] B. Assouar and M. Oudich, Enlargement of a locally resonant sonic band gap by using double-sides stubbed phononic plates, Appl. Phys. Lett. **100**, 123506 (2012).

[16] J. C. Hsu and T. T. Wu, Lamb waves in binary locally resonant phononic plates with two-dimensional lattices, Appl. Phys. Lett. **90**, 201904 (2007).

[17] J. H. Oh, Y. E. Kwon, H. J. Lee, and Y. Y. Kim, Elastic metamaterials for independent realization of negativity in density and stiffness, Sci. Rep. **6**, 23630 (2016).

[18] J. H. Oh, H. M. Seung, and Y. Y. Kim, Adjoining of negative stiffness and negative density bands in an elastic metamaterial, Appl. Phys. Lett. **108**, 093501 (2016).

[19] A. Bergamini, T. Delpero, L. D. Simoni, L. D. Lillo, M. Ruzzene, and P. Ermanni, Phononic crystal with adaptive connectivity, Adv. Mater. **26**, 1343 (2014).

[20] R. Zhu, X. N. Liu, G. K. Hu, C. T. Sun, and G. L. Huang, Negative refraction of elastic waves at the deep-subwavelength scale in a single-phase metamaterial, Nat. Commun. **5**, 5510 (2014).

[21] M. Yang, G. Ma, Z. Yang, and P. Sheng, Coupled Membranes with Doubly Negative Mass Density and Bulk Modulus, Phys. Rev. Lett. **110**, 134301 (2013).

[22] G. Ma, C. Fu, G. Wang, P. Hougne, J. Christensen, Y. Lai, and P. Sheng, Polarization bandgaps and fluid-like elasticity in fully solid elastic metamaterials, Nat. Commun. **7**, 13536 (2016).

[23] G. Ma and P. Sheng, Acoustic metamaterials: From local resonances to broad horizons, Sci. Adv. **2**, e1501595 (2016).

[24] Y. Liu, Z. Liang, F. Liu, O. Diba, A. Lamb, and J. Li, Source Illusion Devices for Flexural Lamb Waves Using Elastic Metasurfaces, Phys. Rev. Lett. **119**, 034301 (2017).

[25] J. Mei, G. Ma, M. Yang, Z. Yang, W. Wen, and P. Sheng, Dark acoustic metamaterials as super absorbers for low-frequency sound, Nat. Commun. **3**, 756 (2012).

[26] Y. Li and B. Assouar, Acoustic metasurface-based perfect absorber with deep subwavelength thickness, Appl. Phys. Lett. **108**, 063502 (2016).

[27] J. Li, W. Wang, Y. Xie, B. I. Popa, and S. A. Cummer, A sound absorbing metasurface with coupled resonators, Appl. Phys. Lett. **109**, 091908 (2016).

[28] M. Yang, S. Chen, C. Fu, and P. Sheng, Optimal sound-absorbing structures, Mater. Horiz. **4**, 673 (2017).

[29] Y. Li, S. Qi, and B. Assouar, Theory of metascreen-based acoustic passive phased array, New J. Phys. **18**, 043024 (2016).

[30] S. Qi, M. Oudich, Y. Li, and B. Assouar, Acoustic energy harvesting based on a planar acoustic metamaterial, Appl. Phys. Lett. **108**, 263501 (2016).

[31] J. H. Oh, H. M. Seung, and Y. Y. Kim, A truly hyperbolic elastic metamaterial lens, Appl. Phys. Lett. **104**, 073503 (2014).

[32] S. H. Lee, C. M. Park, Y. M. Seo, Z. G. Wang, and C. K. Kim, Acoustic metamaterial with negative density, Phys. Lett. A **373**, 4464 (2009).

[33] S. H. Lee, C. M. Park, Y. M. Seo, Z. G. Wang, and C. K. Kim, Acoustic metamaterial with negative modulus, J. Phys. Condens. Matter **21**, 175704 (2009).

[34] D. Yu, J. Wen, H. Shen, Y. Xiao, and X. Wen, Propagation of flexural wave in periodic beam on elastic foundations, Phys. Lett. A **376**, 626 (2012).

[35] S. Yao, Z. Zhou, and G. Hu, Investigation of the negative-mass behaviors occurring below a cut-off frequency, New J. Phys. **12**, 103025 (2010).

[36] C. Yilmaz, G. M. Hulbert, and N. Kikuchi, Phononic band gaps induced by inertial amplification in periodic media, Phys. Rev. B **76**, 054309 (2007).

[37] S. Taniker and C. Yilmax, Design, analysis and experimental investigation of three-dimensional structures with inertial amplification induced vibration stop bands, Int. J. Solids Struct. **72**, 88 (2015).

[38] G. Acar and C. Yilmaz, Experimental and numerical evidence for the existence of wide and deep phononic gaps induced by inertial amplification in two-dimensional solid structures, J. Sound Vib. **332**, 6389 (2013).

[39] N. M. M. Frandsen, O. R. Bilal, J. S. Jensen, and M. I. Hussein, Inertial amplification of continuous structures: Large band gaps from small masses, J. Appl. Phys. **119**, 124902 (2016).

[40] S. Taniker and C. Yilmaz, Generating ultra wide vibration stop bands by a novel inertial amplification mechanism topology with flexure hinges, Int. J. Solids Struct. **106–107**, 129 (2017).

[41] J. H. Oh and B. Assouar, Quasi-static stop band with flexural metamaterial having zero rotational stiffness, Sci. Rep. **6**, 33410 (2016).

[42] S. J. Choi, Master's dissertation, Seoul National University, 2016.

[43] K. F. Graff, *Wave Motion in Elastic Solids* (Dover, New York, 1991).

[44] See Supplemental Material at http://link.aps.org/supplemental/10.1103/PhysRevApplied.8.054034 for the details of analytic, numerical, and experimental procedures.

[45] L. Meirovitch, *Fundamentals of Vibrations* (McGraw-Hill, New York, 2012).

[46] P. Langlet, A.-C. Hladky-Hennion, and J.-N. Decarpigny, Analysis of the propagation of plane acoustic waves in passive periodic materials using the finite element method, J. Acoust. Soc. Am. **98**, 2792 (1995).